7556 *Biochemistry* **2009,** *48,* 7556–7564
DOI: 10.1021/bi900805s

BIOCHEMISTRY
including biophysical chemistry & molecular biology
Article

Mechanism of Ligand-Induced Folding of a Natively Unfolded Helixless Variant of Rabbit I-BABP[†]

Anita M. Rea, Victoria Thurston, and Mark S. Searle*

School of Chemistry, Centre for Biomolecular Sciences, University Park, University of Nottingham, Nottingham NG7 2RD, U.K.

Received May 11, 2009; Revised Manuscript Received June 25, 2009

ABSTRACT: Substitution of the helix−turn−helix capping motif (residues 9−35) of rabbit I-BABP with a flexible Gly-Gly-Ser-Gly linker results in the loss of stabilizing hydrophobic contacts and renders the β-clamshell structure of this steroidal bile acid transport protein unfolded. However, in the presence of a bile acid ligand, we observe strong coupling between binding and folding, resulting in an enthalpy-driven high-affinity interaction ($K_A \sim 4 \times 10^5$ M^{-1}) that "rescues" the native state. We investigate the mechanism of induced folding using fluorescence stopped-flow kinetic measurements to distinguish between conformational selection and induced-fit models. We observe both ligand-dependent and -independent kinetic phases which, together with their relative amplitudes, we attribute to an induced-fit "fly casting" type of model in which transient encounter complexes between the ligand and the extended polypeptide chain may act as nucleation sites for folding. An initial fast ligand-dependent kinetic process appears to be consistent with formation of a hydrophobically collapsed intermediate state which slowly rearranges to a nativelike β-clamshell structure. We show that the intermediate forms at a rate 1000 times slower than the rate of ligand association with wild-type I-BABP, reflecting the large configurational entropic barrier to the coupled binding and folding steps of Δα-I-BABP. We have provided mechanistic insights into how natively disordered states, now commonly identified in biology, may fold on binding a target substrate or ligand.

The correlation between protein structure and function has become an axiom in modern biology. However, the identification of proteins which appear to be natively unfolded yet still perform a specific function may require a reassessment of this paradigm (*1*, *2*). Disorder in proteins can range from regions of local random coil to molten globule or fully unfolded states, with unstructured molecules being implicated in transcriptional regulation, translation, and cellular signal transduction among other functions (*2*). A lack of nativelike structural preorganization does not appear to preclude efficient catalysis, as demonstrated by an engineered monomeric mutant of the dimeric chorismate mutase (*3*). In many cases, it has been observed that the folding of the natively unstructured polypeptide chain, or a partially structured state, is coupled to a ligand binding event (*4*). The phosphorylated kinase-inducible domain (pKID) of the transcription factor cyclic-AMP-response-element-binding protein (CREB) folds upon formation of a complex with the KID-binding (KIX) domain of CREB-binding protein (CBP) (*5*, *6*). The entropic cost of ordering the natively unfolded chain suggests that such coupled binding and folding events are necessarily driven by strongly enthalpic contributions. In addition to natively unfolded proteins, engineered variants with reduced stability have also been shown in some cases to exist in a disordered state under otherwise native conditions yet are still capable of normal biological function (*7*−*10*). Oncogenic mutations in tumor suppressor p53 have been shown to result in a loss of native structure at body temperature, impairing function and promoting aggregation. Designed "rescue ligands" are able to induce the formation and stabilization of the native state of oncogenic p53 mutants with destabilizing surface lesions, ensuring that the protein can reach the cell nucleus and attach to its DNA target (*11*−*13*).

In this context, we have recently described a helixless variant of rabbit I-BABP[1] (Δα-I-BABP), a 10-stranded β-clamshell structure involved in the transport and enterohepatic circulation of bile acids (*14*−*20*). Substitution of the helix−turn−helix capping motif (residues 9−35) with a flexible Gly-Gly-Ser-Gly linker (Figure 1c) renders the protein highly unfolded (*21*), in contrast to earlier related studies on other lipid binding protein family members that remain folded (*22*−*27*). However, bile acid ligands bind with high affinity to Δα-I-BABP by inducing the polypeptide chain to assemble into a nativelike state forming a 1:1 protein−ligand complex. In contrast, multiple ligand binding sites are detected with wild-type I-BABP (*wt*-I-BABP) (up to 3:1) (*21*), which is evident from both ITC and mass spectrometry, with two of the bile acid molecules bound highly cooperatively within the central cavity of the β-clamshell fold (*28*−*31*).

Our observations to date with Δα-I-BABP indicate that the mutant shows a significant degree of disorder under conditions in which the *wt*-I-BABP forms a stable fold. Despite the significant destabilization of the native folded state, bile acid ligands bind with high affinity ($K_a > 10^5$ M^{-1}) without a large thermodynamic "cost" associated with inducing folded structure in

[†]We thank the BBSRC of the U.K. and the School of Chemistry, University of Nottingham, for funding.

*To whom correspondence should be addressed. E-mail: mark.searle@nottingham.ac.uk. Telephone: (44) 115 951 3567. Fax: (44) 115 846 6059.

[1]Abbreviations: I-BABP, ileal bile acid binding protein; Δα-I-BABP, helixless variant of ileal bile acid binding protein; I-FABP, intestinal fatty acid binding protein; TCDC, taurochenodeoxycholate; PDB, Protein Data Bank.

 Published on Web 07/06/2009

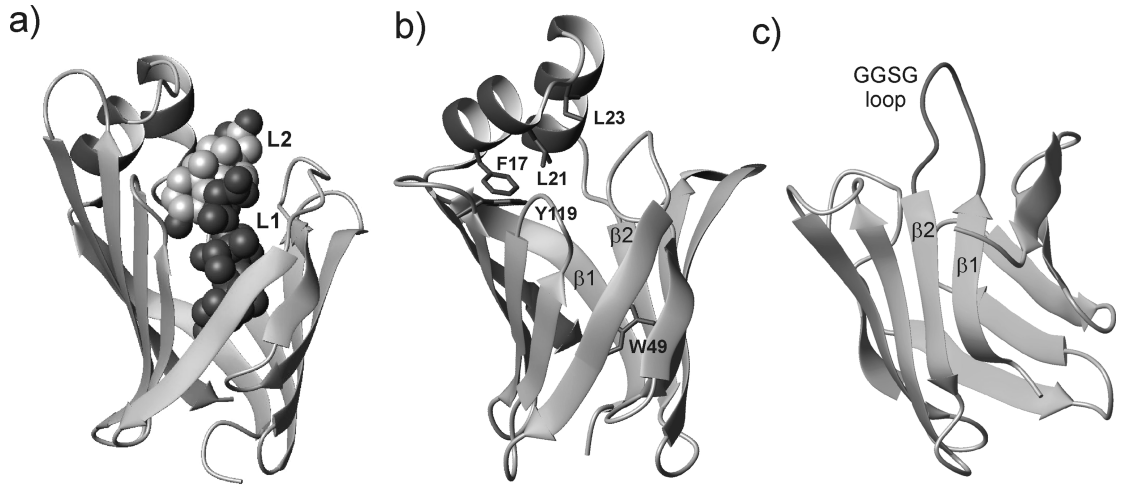

FIGURE 1: (a) Relative orientation of two cholic acid ligands (L1 and L2) bound in the cavity of zebrafish I-BABP showing contacts between ligand L2 (lighter gray) and the helical capping motif, while L1 (darker gray) is buried within the pocket (PDB entry 3ELX). (b) Structural model of rabbit I-BABP based upon the NMR structure of the human variant (PDB entry 101U) showing the side chains on helix 1 and on the adjacent loop that were mutated to Ala to probe stability; in addition, the F17−Y119 interaction is highlighted, as is the position of W49 within the binding cavity. Strands β1 and β2 are connected through the helix capping motif (residues 9−35). (c) Model of the structure of Δα-I-BABP derived from the same coordinates (101U) by substitution of the helical capping motif (residues 9−35) with a flexible Gly-Gly-Ser-Gly linker between strands β1 and β2. The structure is rotated ∼180° with respect to that in panel b.

Δα-I-BABP (*10*, *21*). In this study, we investigate the mechanism by which the two events (folding and binding) are linked using stopped-flow kinetic experiments monitored by tryptophan fluorescence. Two kinetic phases (k_{fast} and k_{slow}) are distinguished on the basis of their ligand concentration dependence and were examined in the context of both induced-fit and conformational selection models that are mechanistically distinct in terms of the order of rapid ligand association and slower conformational rearrangement (*7*, *32*, *33*). We demonstrate that a "binding before folding" model appears to account for the experimental data and propose an induced-fit type of mechanism involving an initially rapid and transient interaction of the ligand with a disordered state that induces hydrophobic collapse of the polypeptide chain followed by a slow conformational rearrangement as the chain descends the folding funnel toward a nativelike state.

MATERIALS AND METHODS

Preparation of Materials. Bile acids and other reagents were purchased from Sigma-Aldrich (Poole), unless otherwise stated. All the experiments were conducted in a buffer solution containing either 20 mM Na_2HPO_4/NaH_2PO_4 and 100 mM NaCl (pH 7.2) or in the case of stopped-flow and CD studies at pH 5 20 mM sodium acetate and 100 mM NaCl. Gene cloning and mutagenesis were conducted as previously described (*21*). The pSGAT2-His_6-Thr-I-BABP construct was transformed into $CaCl_2$-competent *Escherichia coli* BL21(DE3) cells. For purification of His_6-Thr-I-BABP, 1 mL gravity flow Talon columns were used equilibrated with IMAC buffer. Recovered fractions were then analyzed by SDS−PAGE, pooled, and spin concentrated to 5 mL using Vivaspin 20K 3 kDa cutoff 20 mL spin columns. This solution was passed down a Superdex 75 gel filtration column (GE Life Sciences, GE Healthcare) using a 100 mM NaCl/30 mM potassium phosphate buffer at pH 7, prior to buffer exchange using a HiTrap (Amersham, Pharmacia) desalting column. Fractions containing pure protein were pooled, spin concentrated and snap frozen in liquid N_2, and stored at −80 °C. The construct pSGAT2-His_6-Thr-Δα-I-BABP was transformed into *E. coli* BL21 cells. The mutant protein was expressed initially in an insoluble form. The protein was pelleted (30000*g* for 20 min at 4 °C) and the supernatant removed. The pellet was dissolved in 15 mL of IMAC buffer with 7 M urea and purified using the same 1 mL Talon gravity flow column described above (*21*). The concentration of the protein was maintained at less than 1 mg/mL; otherwise, the protein began to precipitate. At concentrations of freshly prepared protein (*wt*-I-BABP and Δα-I-BABP) below ∼1 mg/mL, we see no evidence of significant concentration-dependent effects on CD and NMR spectra.

NMR, CD, Fluorescence, DSC, and ITC Studies. NMR data were collected at 600 MHz on a Bruker Avance600 spectrometer equipped with a triple-resonance inverse-detection probe and z-field gradients. Samples of 0.1−0.5 mM were prepared in 600 μL of aqueous buffer [20 mM Na_2HPO_4/NaH_2PO_4 and 100 mM NaCl (pH 7.2)] at 298 K. Binding and protein stability studies were performed by monitoring Trp fluorescence emission on a Perkin-Elmer L550B fluorimeter. Data were collected between 310 and 380 nm with an excitation wavelength of 283 nm. The bile acids were dissolved in buffer at pH 7.2 or 5.0 at a high concentration (20−40 mM). Two solutions of 1 μM protein in 2 mL of the same buffer were prepared. One solution was used as a control, and in the other, the bile acid stock solution was added to give a final ligand concentration of 200 μM, representing a 200-fold excess of ligand to ensure saturated binding. A total of 10 scans were recorded at 298 K in a thermostated water bath; these were averaged and solvent subtracted. CD spectra were collected on an Applied PhotoPhysics Pistar system at protein concentrations between 15 and 30 μM in 20 mM Na_2HPO_4/NaH_2PO_4 (pH 7). In all cases, the spectrum corresponding to buffer alone was recorded and subtracted from sample spectra. The sample was read in a cuvette with a path length of 1 mm. Secondary structure content was investigated by recording spectra between 200 and 250 nm in 1 nm steps with 4.0−6.0 nm entrance and exit slit widths. VP-ITC and VP-DSC high-sensitivity isothermal titration and differential scanning calorimeters (MicroCal, Inc.) were used to assess the interaction of bile acid ligands with *wt*-I-BABP and Δα-I-BABP and the thermal stability of the proteins and their complexes following the methodology previously described (*21*).

Stopped-Flow Fluorescence Kinetics. Stopped-flow fluorescence data were also collected on the Pistar system with the temperature regulated by a Neslab RTE-300 circulating water bath with a temperature controller. Fluorescence-monitored kinetic studies were conducted at 298 K in 20 mM sodium acetate buffer and 150 mM NaCl (pH 5). Rapid mixing experiments were performed by 1:10 dilution of unbound protein (15 μM) into buffered solutions of different bile acid concentrations, yielding a final protein concentration of 1.36 μM. Control dilution experiments in buffered solutions without ligand present produced no observable change in fluorescence or any detectable kinetic process. Kinetic measurements were averaged four to six times at each bile acid concentration. Complete sets of fluorescence curves for the binding of bile acid to *wt*-I-BABP were globally analyzed using Dynafit (*34*).

Molecular Modeling. Calculations were performed using a 12 CPU Opteron Cluster running RedHat Linux with MPI support for the sander module of AMBER8 or on workstations using 64-bit Fedora. The starting structure was created by deletion of residues 9−35, and the intervening gap was bridged by a "long" bond of approximately 5 Å. The system was parametrized using the xLEaP module of AMBER8 using the AMBER99 force field (*35*). Charges were neutralized using monovalent ions and explicit solvent added using the TIP3P solvent model with a 9 Å buffer cutoff using truncated octahedral geometry. The model was run using periodic boundary conditions, and electrostatics were calculated using the particle mesh Ewald method. All dynamics calculations use the SHAKE method to remove fast vibrations and employ a 2 fs time step. The system was equilibrated by first steepest decent minimization followed by a conjugate gradient minimization yielding an acceptable initial geometry. The system was then further equilibrated by 100 ps of molecular dynamics using a temperature ramp from 100 to 300 K while removing coordinate restraints in a stepwise maner from 100 kcal mol^{-1} Å^{-2} to 0. The system was then run for 1 ns. Structures were sampled from the last 100 ps, and the ensemble was displayed. A representative structure (based on the root-mean-square deviation) was subjected to energy minimization and displayed using MOLMOL (*36*).

RESULTS

Homology Modeling of Δα*-I-BABP and Protein−Ligand Complexes*. A recent crystallographic structure of zebrafish I-BABP (which shares ~50% sequence homology) has resolved two internally bound cholate molecules (L1 and L2 at sites 1 and 2), and electron density consistent with other surface-bound ligands (*37*). Site 1 is buried deep within the central β-clamshell cavity, while site 2 is located close to the ligand entry portal with extensive ligand contacts with the capping helical motif (Figure 1). ITC and ESI-MS studies of rabbit I-BABP have demonstrated the binding of three bile acid molecules (*21*), but only two of these are located within the cavity, which is also evident for the human variant (*29*, *30*), although a detailed structural analysis has yet to be reported. In contrast to *wt*-I-BABP, the Δα-I-BABP mutant appears to bind only a single bile acid ligand with high affinity (*21*). We have constructed homology models for rabbit *wt*-I-BABP and Δα-I-BABP from the structure of the human form (PDB entry 101U) to rationalize the change in binding stoichiometry that we observe for Δα-I-BABP. Replacement of the helical motif (residues 9−35) with a Gly-Gly-Ser-Gly linker eliminates many side chain contacts with L2 and increases its solvent accessibility. Molecular dynamics simulations over ~1 ns on the Δα-I-BABP model suggested that L2 no longer forms a stable interaction (data not shown), although the strong interactions with L1, including contacts with W49 in the binding cavity, appear to be largely unaffected. Thus, loss of contacts between L2 and residues of the helix capping motif appear to explain the observation of only a single high-affinity binding site for Δα-I-BABP.

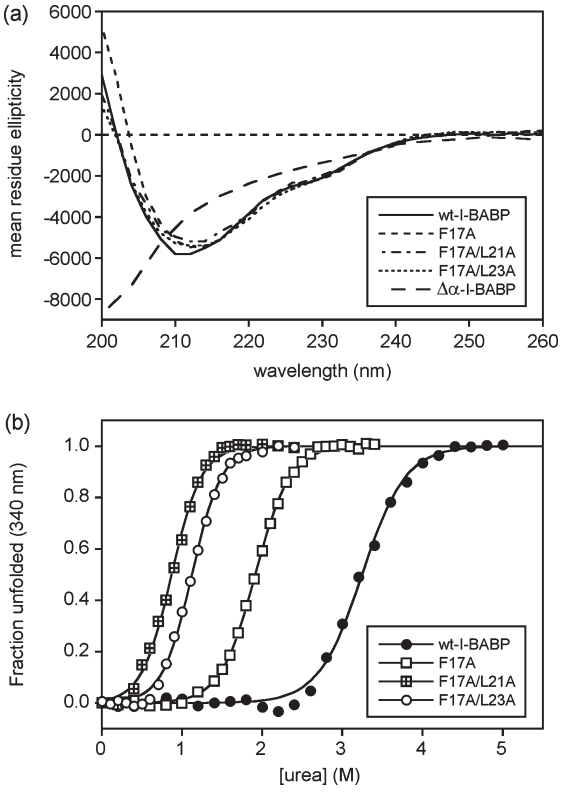

FIGURE 2: (a) CD spectra of *wt*-I-BABP, the Δα-I-BABP mutant, the single-point mutant F17A, and double mutants F17A/L21A and F17A/L23A at 298 K buffered at pH 7.0. (b) Urea-induced denaturation curves for the same mutants at 298 K monitored by W49 fluorescence. Data were converted to fraction folded vs urea concentration (molar), and the change in position of the unfolding midpoint $[urea]_{50\%}$ reflects the effects of the mutation on stability.

Helix Mutations Destabilize wt-I-BABP. We investigated the effects of specific contacts between the helices and the β-clamshell core of the structure to rationalize the observation that Δα-I-BABP is rendered largely unfolded. Indeed, a number of pairwise hydrophobic side chain contacts appear to be highly conserved across this family of β-barrel proteins, suggesting a structural role in stabilizing the protein fold (*14*, *19*, *20*). Specific stabilizing contacts are observed between F17 on helix 1 and I114, V117, and in particular the β-turn residue Y119, which are readily apparent as NOE contacts in solution NMR studies of *wt*-I-BABP (unpublished results) (Figure 1). To test the impact of this contact, and the effects of other buried hydrophobic side chains on helix 1 and the adjacent loop on overall stability, we introduced the F17A mutation and two double Ala mutations (F17A/L21A and F17A/L23A) (Figure 1). Both L21 and L23 also make contacts between the helix capping motif and residues in the loops of the β-clamshell structure (L21 → I114, F74, and F79 and L23 → F74, G75, and G76). By CD, the structure of these mutants is indistinguishable from that of *wt*-I-BABP, indicating no significant loss of secondary or tertiary structure (Figure 2a). However, the impact on stability is pronounced,

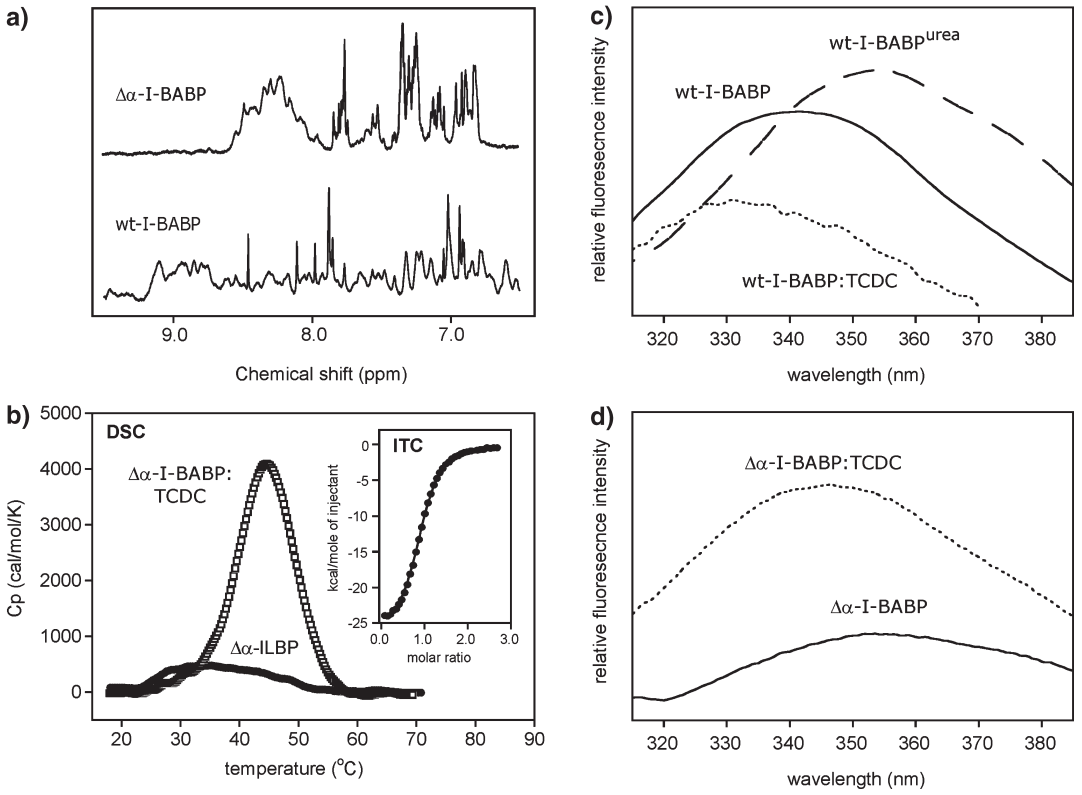

FIGURE 3: (a) ^{1}H NMR spectra at 600 MHz of the NH and aromatic region (6.5−9.5 ppm) of the spectra of *wt*-I-BABP and Δα-I-BABP at 298 K. (b) DSC data for Δα-I-BABP and the complex of Δα-I-BABP with TCDC. The unliganded protein shows a broad featureless transition indicative of a disordered unfolded state; however, a cooperative transition is observed for the TCDC−Δα-I-BABP complex with a large enthalpy change, indicating that the ligand induces a structured state in the protein ($T_m \sim 44$ °C). (c) Fluorescence emission spectra for *wt*-I-BABP in the absence of ligand (*wt*-I-BABP), *wt*-I-BABP in the presence of 4 M urea (*wt*-I-BABP^{urea}), and *wt*-I-BABP with TCDC bound in the presence of an excess of bile acid. (d) Fluorescence spectra of Δα-I-BABP and the TCDC complex of Δα-I-BABP.

despite the increase in secondary structure propensity associated with introduction of Ala mutations into the helix. Equilibrium unfolding curves determined from urea denaturation studies monitored by fluorescence show large shifts in the transition midpoints (Figure 2b). For *wt*-I-BABP, this occurs at 3.25 M urea but is shifted to 1.91 M urea for F17A and much further still for the double mutants F17A/L21A (0.87 M) and F17A/L23A (1.12 M), indicating that these mutants have only marginal stability over the unfolded state at 298 K in aqueous buffer. Thermal unfolding studies of the mutants monitored by CD at 214 nm show ~30 K reductions in thermal stability compared with *wt*-I-BABP, with transition regions of the sigmoidal melting curves extending below 298 K (not shown), indicating that these destabilized mutants are at least partially unfolded at this temperature. Thus, the loss of hydrophobic contacts between the helical motif and the rest of the protein appears to rationalize the observation that complete removal of the helical capping motif renders Δα-I-BABP "natively unfolded".

NMR and Fluorescence Studies of the Natively Unfolded State of Δα-I-BABP. Defining a structural model of the natively unfolded state of Δα-I-BABP is more challenging. NMR spectra at 600 MHz were recorded for *wt*-I-BABP and Δα-I-BABP at 298 K in phosphate buffer at a protein concentration of 0.1−0.5 mM (Figure 3a). The abundance of slowly exchanging NH resonances observed for *wt*-I-BABP, with a wide chemical shift dispersion (6.5−9.0 ppm), is characteristic of a globular protein structure. In contrast, the NH chemical shift dispersion for the Δα-I-BABP mutant is much narrower (8.0−8.5 ppm), indicative of a substantial loss of native structure. Moreover, signals from the aromatic nonexchangeable protons, and some methyl signals, are particularly sharp with a number of *J* splittings readily resolved and indicative of rapid side chain and backbone dynamics. These conclusions are supported by previously reported CD data (*10*) which show a weakening of the band at 216 nm corresponding to β-sheet structure, but a much more negative ellipticity at 200 nm for Δα-I-BABP, indicative of an increase in the level of flexible, disordered structure. Thus, although the data suggest a substantial loss of stable nativelike hydrogen bonded secondary structure, the degree of residual structure in the disordered polypeptide chain remains to be characterized in detail.

NMR provides a global picture of secondary and tertiary interactions within the polypeptide chain, whereas tryptophan fluorescence can identify local side chain contacts consistent with residual structure in the unfolded state and local nuclei of hydrophobic collapse. The single tryptophan (W49) in *wt*-I-BABP is a key residue located at the base of the ligand binding cavity in the native folded structure and has been shown to undergo large changes in fluorescence associated with both ligand binding and protein folding (*21*). Fluorescence emission spectra for *wt*-I-BABP at pH 5.0 in aqueous buffer and denatured in 4 M urea are shown in Figure 3c, with the λ_{max} of the denatured state showing the characteristically enhanced signal intensity and a shift from 340 to 355 nm. In contrast, the spectrum of Δα-I-BABP shows a λ_{max} of 353 nm (Figure 3d), comparable to that of the urea-unfolded state of *wt*-I-BABP. Chemical denaturation of Δα-I-BABP in ≤4 M urea leads to only a small additional change in fluorescence intensity and shift in

the λ_{max} of ~355 nm, suggesting that Δα-I-BABP is already in a largely denatured state.

Interaction of TCDC with Δα-I-BABP. Both mass spectrometry (ESI-MS) and ITC techniques had indicated that the taurine-conjugated chenodeoxycholate (TCDC) binds to rabbit Δα-I-BABP with the highest affinity of the three taurine-conjugated bile acids studied (*21*) and is the focus of our current investigations. DSC and ITC data for the interaction of Δα-I-BABP with TCDC are shown in Figure 3b. The DSC melt for Δα-I-BABP shows no discernible features, indicative of the absence of a cooperative unfolding transition and an ensemble of disordered structures. However, in the presence of TCDC, we see a pronounced thermal unfolding curve for Δα-I-BABP (T_m ~ 44.5 °C) associated with a large enthalpy change at the transition midpoint, typical of a cooperative melting process. The inset in Figure 3b shows the ITC titration of Δα-I-BABP with TCDC which produces a sigmoidal binding curve with a well-defined 1:1 binding stoichiometry. The large enthalpy change (−109.5 ± 0.3 kJ mol^{-1}) is clear evidence of a strong coupling between folding and binding since ligand binding to *wt*-I-BABP produces a significantly smaller exothermicity (*21*).

We examined the binding interaction of Δα-I-BABP using intrinsic tryptophan fluorescence in the presence and absence of 500 μM TCDC at pH 5 and 7. The largest change in fluorescence was detected at pH 5.0 (Figure 3d), with TCDC causing a sizable enhancement in the intensity, in contrast to the net fluorescence quenching observed for this ligand with *wt*-I-BABP. The binding of TCDC produces a substantial blue shift (λ_{max} = 346 nm) and enhancement of fluorescence intensity, indicative of the ligand-induced folding of Δα-I-BABP also apparent in earlier CD measurements (*10*, *21*). Thus, to maximize the signal-to-noise ratio in kinetic experiments using stopped-flow fluorescence, we worked at pH 5.0.

The amplitude of the fluorescence change associated with interaction of the ligand with Δα-I-BABP is worthy of note because the overall effect appears to be different from those predicted from the behavior of *wt*-I-BABP. The coupled effects of folding and binding were first considered on the basis of observations made for *wt*-I-BABP with TCDC. Refolding of *wt*-I-BABP from 4 M urea is also shown in Figure 3c and is associated with the quenching of fluorescence intensity as the indole side chain becomes less solvent exposed. Subsequently, the binding of TCDC to the native *wt*-I-BABP also produces an additional quenching of fluorescence intensity, likely associated with the expulsion of residual solvent molecules from the binding cavity to accommodate two bile acid molecules. Thus, the *wt*-I-BABP−TCDC complex is significantly less fluorescent than the denatured state of *wt*-I-BABP with additive reductions associated with first the folding and then the binding steps. This analysis contrasts with the observation of the effect of TCDC on the fluorescence intensity of Δα-I-BABP. In equilibrium binding studies, we see a single large fluorescence enhancement associated with coupled folding and binding events. One possible conclusion is that the more open binding cavity of the complex of Δα-I-BABP with a single, as opposed to multiple, site occupancy permits solvent molecules to be bound in the proximity of the indole side chain. The high-resolution structure of zebrafish I-BABP with two cholate molecules accommodated in the binding cavity also readily identifies at least five well-defined solvent molecules mediating interactions between protein and ligands (*37*), as have previously published structures of homologous fatty acid binding proteins (*38*, *39*).

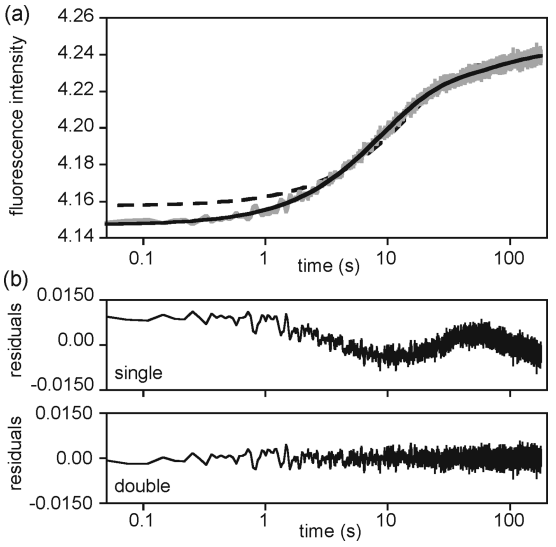

FIGURE 4: Stopped-flow kinetic data for TCDC binding to Δα-I-BABP at 283 K. Protein (15 μM) was rapidly mixed and diluted 10-fold with an excess of ligand. The fluorescence enhancement with time is fitted to both a single exponential (– – –) and a double exponential (—). Residuals for the two fits are shown in panel b with the double-exponential fit appearing to account well for the fluorescence decay curve.

Mechanism of Ligand-Induced Folding of Δα-I-BABP. We conducted stopped-flow fluorescence experiments to investigate the mechanism of binding of TCDC to Δα-I-BABP. The increase in intrinsic protein fluorescence was recorded upon rapid mixing of varying concentrations of TCDC all in an identically buffered solution [150 mM NaCl and 20 mM sodium acetate (pH 5.0, 298 K)]. All kinetic traces were described well by a double exponential which resulted in small random residuals (Figure 4). The two kinetic phases (k_{slow} and k_{fast}) showed different ligand concentration dependencies. The faster of the two phases showed rate constants with a linear dependence on TCDC concentration, while the slower of the two rates showed little dependence (Figure 5a). The amplitudes of both phases also showed a linear increase with an increase in ligand concentration (Figure 5b).

When a ligand binding event is characterized by one fast ligand association step and one slow step, two distinct mechanistic possibilities arise, particularly in the case when the protein component is highly unfolded. The two possible mechanisms broadly differentiate between the sequence of events that have been described as folding before binding or binding before folding but are more familiar as the conformational selection or an induced-fit model (*32*, *33*). In the conformational selection model, preferential binding of a ligand occurs to a high-affinity conformational subpopulation (P*), which is present at equilibrium with the natively unfolded state (P), resulting in the formation of the thermodynamically stable complex P*L (*40*). The unbound protein (P) is assumed to sample a number of conformations, and a high-affinity excited state (P*) selectively binds the ligand. As the ligand concentration increases, the binding interaction with P* shifts the equilibrium toward the fully bound state (P*L). In contrast, the induced-fit model involves the ligand binding to the unfolded conformation (P) to nucleate formation of a compact protein−ligand intermediate, which subsequently undergoes a slow conformational rearrangement as this partially folded state descends the folding funnel toward a nativelike structure (*41*).

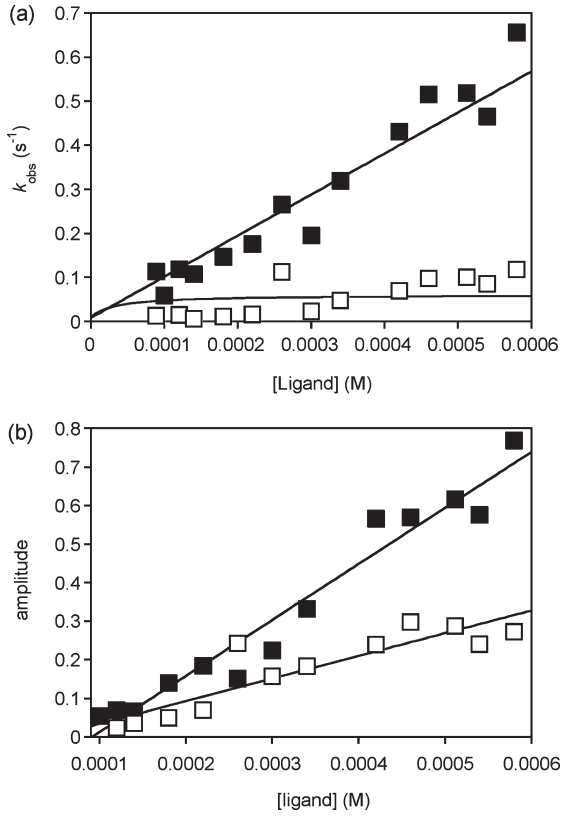

FIGURE 5: (a) Change in rate constants as a function of ligand concentration for the two kinetic phases identified in Figure 4. The faster phase shows a clear ligand concentration dependence, whereas the slower phase is largely independent of ligand concentration. The data were fitted according to the model for induced-fit ligand binding described in the text. The relative amplitudes of the two kinetic phases are also shown with both demonstrating a linear correlation with ligand concentration.

Each of these models has well-defined kinetic characteristics (*32*, *42*). The conformational selection process, summarized in the following equilibrium, is defined by a slow protein conformational change (k_{slow}), followed by a rapid ligand binding step (k_{fast}):

$$P \underset{k_{-1}}{\overset{k_1}{\rightleftharpoons}} P^* + L \underset{k_{-2}}{\overset{k_2}{\rightleftharpoons}} P^*L$$

The two kinetic processes have the following dependence on [L], showing a linear dependence for k_{fast}, but nonlinear dependence for k_{slow}:

$$k_{slow} = k_1 + k_{-1}/[1 + [L]/(k_{-2}/k_2)]$$

$$k_{fast} = k_{-2} + k_2[L]$$

In this case, an asymptotic decrease in k_{slow} is predicted since k_{slow} is inversely dependent on [L], leading to a depletion of the population of P* and a limiting value of $k_{slow} \sim k_1$ (*32*, *42*). Although there is some scatter in the data, a decrease in k_{slow} is not readily apparent. In addition, we find that the amplitude of k_{slow} increases linearly with [TCDC], whereas in the conformational selection model, the amplitude would be expected to be largely invariant with ligand concentration. The substantial amplitude of the slower phase seen in Figure 4b suggests a large flux of folding molecules, with P* already significantly populated. The NMR data for Δα-I-BABP showed little evidence of a significant population of partially folded molecules that could match the amplitudes observed in the kinetic studies. Despite our observations, examples of this model exist in the literature and have been described for the binding of a native disordered staphylococcal nuclease mutant monitored by CD stopped-flow methods (*32*).

We subsequently attempted to fit the variation in observed rate constants with increasing ligand concentration to an induced-fit model (*7*, *32*, *42*), assuming the following scheme:

$$P + L \underset{k_{-1}}{\overset{k_1}{\rightleftharpoons}} PL \underset{k_{-2}}{\overset{k_2}{\rightleftharpoons}} P^*L$$

In this case k_{slow} and k_{fast} are defined as follows:

$$k_{slow} = k_{-2} + k_2[L]/([L] + k_{-1}/k_1)$$

$$k_{fast} = k_{-1} + k_1[L]$$

The results of this analysis can be seen in Figure 5. In both cases, the intercepts (k_{-1} and k_{-2}) are rather poorly defined because of the scatter in the data close to the origin. Since k_{-1} and k_{-2} influence the overall equilibrium constant for binding, we fitted the data constrained by the results of the ITC measurements with a $K_{eq} = 3.6 \pm 0.05 \times 10^5$ M^{-1} (Figure 3b). A linear plot of k_{fast} versus [L] yielded a slope and intercept corresponding to k_1 and k_{-1}, respectively. When k_{slow} is considered, we can see that at high ligand concentrations ($[L] > k_{-1}/k_1$) we would predict that the rate is independent of ligand concentration ($k_{slow} \sim k_{-2} + k_2$).

Here, k_{slow} is the sum of the two rate constants for the conformational interconversion between PL and P*L. In the context of Δα-I-BABP, in the induced-fit model, $k_2 > k_{-2}$ since CD and NMR studies both indicate a substantial population of nativelike folded protein in the ligand-bound complex from which we estimated that $k_2 \geq 5k_{-2}$. Although there is some uncertainty in k_{-1} and k_{-2}, the analysis is consistent with the induced-fit model in which ligand binds rapidly, inducing a hydrophobic collapse of the polypeptide chain characterized by a k_1 of $\sim 930 \pm 100$ M^{-1} s^{-1}. Subsequently, a much slower ($k_2 \sim 0.05$ s^{-1}) conformational reorganization occurs to a nativelike folded state. Within the restraints described, we can place an upper limit on the equilibrium association constant K_1 of k_1/k_{-1} ($\sim 10^5$ M^{-1}), consistent with substantial hydrophobic surface burial in formation of the collapsed protein−ligand intermediate.

Ligand Binding to wt-I-BABP. Mechanistic insights into ligand association with *wt*-I-BABP were investigated using a similar approach, following the methodology recently described for human I-BABP by Toke *et al.* (*43*). Protein was rapidly mixed with ligand under pseudo-first-order conditions in which the bile acid is in excess. The binding of bile acid ligands to *wt*-I-BABP resulted in a well-resolved change in the fluorescence of W49. At low ligand concentrations (< 40 μM), the kinetic trace fits to a single exponential; however, at > 40 μM, the data could be fit to a double exponential, including a low-amplitude slow phase of > 1 s^{-1}. Kinetic experiments were repeated at ligand concentrations between 10 and 70 μM, and the dependence of the rate constants on ligand concentration was investigated. Representative traces over a range of ligand concentrations are illustrated in Figure 6a together with the fits from the global analysis using Dynafit. The dominant kinetic phase (k_{obs1}) at pH 5.0 shows an initial decrease in rate constant and then a linear increase with ligand concentration in a manner consistent with

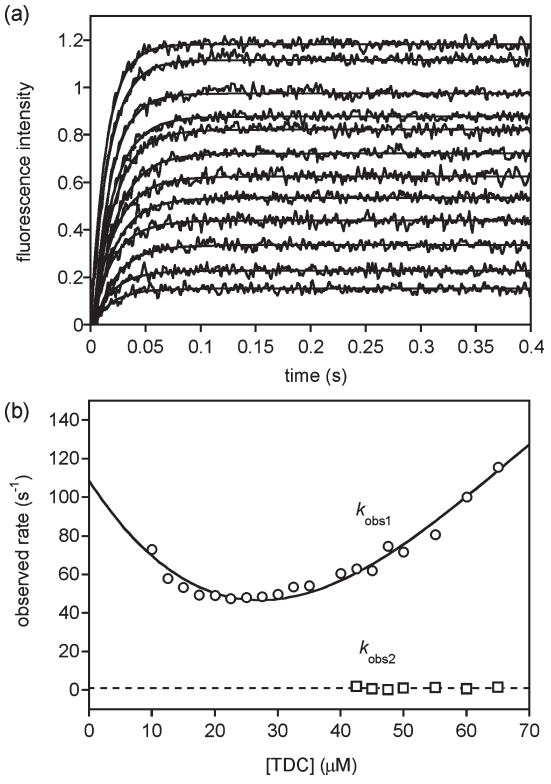

FIGURE 6: Stopped-flow kinetic data for bile acid binding to rabbit *wt*-I-BABP. (a) Variation in the fluorescence amplitude of kinetic traces at different ligand concentrations ranging from 10 to 70 μM, in the presence of 1.3 μM *wt*-I-BABP at 283 K and pH 5. The solid lines represent the best fits to the data. A biexponential fit is required at >40 μM ligand. (b) Variation of the rate constants with ligand concentration shows that the faster phase (k_{obs1}) has a clear dependence; however, the slower second phase (k_{obs2}) appears to be independent of ligand concentration.

a multistep binding process (Figure 6b). The linear portion of the curve of the dependence of k_{obs1} on ligand concentration gives an estimate of the rate of association in the first binding step (k_1) of $\sim$1.3 μM^{-1} s^{-1}. Fitting k_{obs1} to a two-step process using a quadratic function for the dependence on ligand concentration shows that one of the binding steps is associated with a negative amplitude change, consistent with equilibrium binding studies that suggest that the first ligand associates with a quenching of fluorescence intensity. However, the signal-to-noise ratio at very low ligand concentrations (<10 μM) in stopped-flow experiments, together with the high cooperativity in binding two ligands (*28*−*31*, *43*), does not permit us to resolve this first kinetic event in isolation. The low-amplitude slow phase (k_{obs2}), visible at pH 5.0 at >40 μM ligand, appears to be independent of ligand concentration with a k_{obs2} of $\sim$1 s^{-1}. This phase also correlates with a slow process rate-limited by conformational changes in the protein structure which by analogy with Δα-I-BABP appears to occur after both ligands have entered the cavity. In practice, it proved to be difficult to model this slow phase unambiguously because of its low amplitude. Previous work with human I-BABP identified a similar slow minor phase which they attributed to a structural transition occurring after the main ligand binding events (*43*). They also modeled the data with a further unimolecular fast opening event that allows the ligands access to the cavity.

In our global analysis, we considered the following model based upon the behavior of the two distinct kinetic phases, with k_{obs1} described by a quadratic involving step 1 (k_1 and k_{-1}) and step 2 (k_2 and k_{-2}), with k_3 and k_{-3} describing the slow unimolecular event (step 3) which is assumed to take place after both ligands are bound:

$$\text{step 1} \quad P + L \underset{k_{-1}}{\overset{k_1}{\rightleftharpoons}} PL$$

$$\text{step 2} \quad PL + L \underset{k_{-2}}{\overset{k_2}{\rightleftharpoons}} PL_2$$

$$\text{step 3} \quad PL_2 \underset{k_{-3}}{\overset{k_3}{\rightleftharpoons}} P^*L_2$$

Analysis of the data at pH 5.0 and 298 K yields a k_1 of $\sim 1.3 \pm 0.1$ μM^{-1} s^{-1} and a k_2 of $\sim 22 \pm 3$ μM^{-1} s^{-1}, a slow initial binding event and a faster second event reflecting the positive cooperativity between sites, followed by a slow unimolecular event on a time scale k_3 of $\sim 1.3 \pm 0.3$ s^{-1}. These rate constants are consistent with those reported from detailed kinetic studies of human *wt*-I-BABP with a number of different bile acid ligands (*43*). In the context of uncertainties in k_{-1} and k_{-2} derived from the kinetic analysis of rabbit *wt*-I-BABP described here, estimated equilibrium binding constants for each ligand association step are qualitatively consistent with a cooperative binding model in which the affinity at step 2 is enhanced over that of step 1. More complex models, in which a third ligand binding event is accommodated, or an initial fast "opening" phase (*43*), produced large fitting errors with uncertainties in the relative fluorescence of the partially ligated states. In contrast to the data for Δα-I-BABP, ligand binding in step 1 to the preorganized cavity of *wt*-I-BABP appears to be $\sim$1000 times faster than the rate of ligand-induced collapse of Δα-I-BABP ($k_1 \sim 1.3 \pm 0.1$ μM^{-1} s^{-1} vs $k_1 \sim 930 \pm 100$ M^{-1} s^{-1}), consistent with a large kinetic barrier to folding of Δα-I-BABP presumably linked to the large change in configurational entropy associated with polypeptide chain collapse.

DISCUSSION

Coupling the Thermodynamics of Binding and Folding. The induced-fit mechanism of binding was first suggested by Koshland to describe the transition from one tight ensemble of amino acid chain conformations to another upon binding of a ligand molecule (*44*). The fly casting model (*45*, *46*) is a more recent variation offering a mechanistic description of ligand binding to a disordered protein structure in which a flexible unfolded region of the polypeptide chain is "cast out" to weakly and nonspecifically bind the target ligand. Once the ligand has been transiently captured, the polypeptide chain can begin to fold to its free energy minimum, essentially "reeling in" the ligand toward the cognate binding site. Recent work by Sugase *et al.* (*6*) has shown that this mechanism mediates the binding of the pKID domain of the gene transcription factor CREB and the KIX domain of the CREB binding protein. A four-step binding model is suggested [free ↔ encounter ↔ intermediate ↔ bound (F ↔ E ↔ I ↔ B)] whereby the natively unfolded pKID rapidly forms encounter complexes with the KIX domain mediated by non-native contacts. However, measurable kinetics and relaxation effects arise only from the interconversion of the encounter complexes to an intermediate state, such that the steady state interconversion (F ↔ E ↔ I) is replaced with a single-step kinetic process with effective on and off rates for formation of the

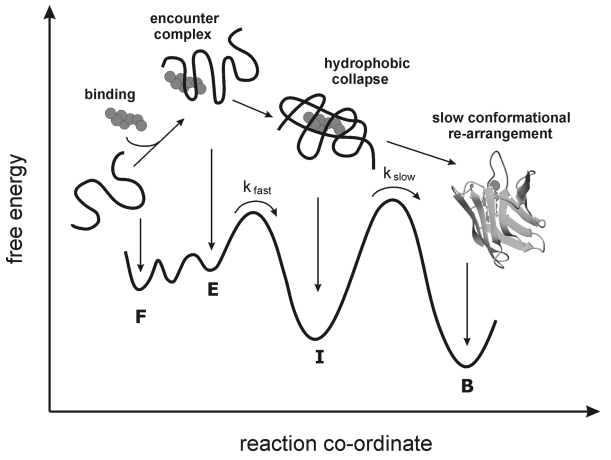

FIGURE 7: Schematic representation of the fly casting model for the binding and folding of Δα-I-BABP in the presence of a bile acid ligand. The four states are as follows: F for free (unbound protein), E for encounter complex, I for intermediate bound state, and B for bound "nativelike" state. The fast phase detected experimentally correlates with ligand-induced hydrophobic collapse of the polypeptide chain and corresponds to the pseudo-single-step process F ↔ E ↔ I. The initial encounter complexes are high in energy and only transiently populated but act as nucleation sites around which the polypeptide chain can fold. The final slow kinetic phase results from the rearrangement of the I state to a nativelike bound state.

intermediate (k_{on}* and k_{off}*, respectively) as regions of its secondary structure become stabilized and specific contacts are formed with the ligand molecule. The measured on rate of ~6×10^6 M^{-1} s^{-1} and the off rate of ~13 s^{-1} result in a binding affinity for the intermediate state of ~5×10^5 M^{-1}. Finally, pKID becomes completely folded as the pKID−KIX domain complex reaches its high-affinity free energy minimum (*6*).

This fly casting model provides a plausible mechanism for the coupled binding and folding of Δα-I-BABP in which the unfolded polypeptide chain has the potential to bind to ligands via nonspecific hydrophobic interactions to yield a rapidly formed ensemble of "encounter" complexes which then act as nucleation sites around which other stabilizing interactions are rapidly formed (Figure 7). By analogy with the analysis of formation of the pKID−KIX complex (*6*), the F ↔ E ↔ I sequence of events can be replaced with a pseudo-single-step process that we are able to observe kinetically. The considerable amount of protein−ligand binding energy ($K_1 \sim 10^5$ M^{-1}) that is realized in the formation of PL in this pseudo-single-step process is comparable to that described for the pKID−KIX complex and is consistent with a collapse of the polypeptide chain and burial of a considerable amount of hydrophobic surface area, even though the initial nucleating encounter complexes are high in energy, are associated with very rapid on and off rates, and are not significantly populated (Figure 7). The intermediate collapsed state (PL) then slowly interconverts to a nativelike complex P*L on a much slower time scale (0.05 s^{-1}) which further consolidates burial of the hydrophobic surface area. However, by analogy to protein folding funnel models (*45*, *47*), transient ligand-bound structures are able to nucleate chain collapse, leading to formation of an intermediate state that is significantly populated and kinetically observable. Our kinetic data resolved two distinct phases, the faster of which showed the ligand concentration dependence consistent with this model.

A Natively Unfolded State by Design. The removal of the helical cap of *wt*-I-BABP leads to a sufficient loss of hydrophobic surface burial between helix and β-sheet as to render the Δα-I-BABP mutant natively unfolded. Indeed, point mutations of hydrophobic residues on helix 1 of *wt*-I-BABP also lead to large destabilizing effects on the protein. However, ligand binding appears to compensate for the structural instability of Δα-I-BABP and "rescues" the native state (*11*−*13*). The mechanism of this process has been described in this study. Binding of bile acids to the preorganized *wt*-I-BABP occurs on a time scale of approximately 1 s, whereas this process is closer to 100 s for Δα-I-BABP. The larger "catch radius" presented by a natively unfolded molecule has previously been reported to increase initial binding rates relative to those of conformationally constrained native states (*45*, *48*). However, we were unable to detect these transient and rapidly formed encounter complexes, only the much slower events involving the ligand-nucleated hydrophobic collapse of the polypeptide chain, and the subsequent slow reorganization to a nativelike state. Capture radius will affect the overall rate of folding only if the initial association of the ligand is rate-limiting, which appears not to be the case in this study. The large entropic barrier derived from the loss of backbone dynamics during hydrophobic collapse of Δα-I-BABP around the "bait" is likely the kinetic determinant for rate-limiting formation of the intermediate protein−ligand complex. Kinetic investigations of the folding mechanism of members of the lipid binding protein family (I-BABP and I-FABP) have provided some insights into differences in the extent of formation of core hydrophobic clusters that drive chain collapse and formation of a kinetic intermediate (*49*). Participating residues from a number of β-strands are implicated in providing a framework for nucleating native secondary structure formation which would also appear to be a competent hydrophobic environment for binding bile acid ligands. We have described an engineered protein system that shows the properties of a natively unfolded state and have provided some mechanistic insight into how such disordered states, now commonly identified in biology, may fold on binding a target substrate.

ACKNOWLEDGMENT

We thank Dr. Nikos Kouvatsos and Prof. Neil Thomas for collaborating on initial DSC and ITC studies on Δα-I-BABP bile acid complexes, Dr. Jill Meldrum for preliminary ligand binding kinetic studies, and Dr. Huw Williams for conducting modeling and MD simulations on ligand complexes of Δα-I-BABP.

REFERENCES

1. Wright, P. E., and Dyson, H. J. (1999) Intrinsically unstructured proteins: Re-assessing the protein structure-function paradigm. *J. Mol. Biol. 293*, 321–331.
2. Wright, P. E., and Dyson, H. J. (2005) Intrinsically unstructured proteins and their functions. *Nat. Rev. Mol. Cell Biol. 6*, 197–208.
3. Vamvaca, K., Vogeli, B., Kast, P., Pervushin, K., and Hilvert, D. (2004) An enzymatic molten globule: Efficient coupling of folding and catalysis. *Proc. Natl. Acad. Sci. U.S.A. 101*, 12860–12864.
4. Dunker, A. K., Brown, C. J., Lawson, J. D., Iakoucheva, L. M., and Obradovic, Z. (2002) Intrinsic disorder and protein function. *Biochemistry 41*, 6573–6582.
5. Radhakrishnan, I.; et al. (1997) Solution Structure of the KIX Domain of CBP Bound to the Transactivation Domain of CREB: A Model for Activator:Coactivator Interactions. *Cell 91*, 741–752.
6. Sugase, K., Dyson, H. J., and Wright, P. E. (2007) Mechanism of coupled folding and binding of an intrinsically disordered protein. *Nature 447*, 1021–1025.
7. Pervushin, K., Vamvaca, K., Vogeli, B., and Hilvert, D. (2007) Structure and dynamics of a molten globular enzyme. *Nat. Struct. Mol. Biol. 14*, 1202–1206.

8. Kohn, J. E., and Plaxco, K. W. (2005) Engineering a signal transduction mechanism for protein-based biosensors. *Proc. Natl. Acad. Sci. U.S.A. 102*, 10841–10845.
9. Koepf, E. K., Petrassi, H. M., Ratnaswamy, G., Huff, M. E., Sudol, M., and Kelly, J. W. (1999) Characterization of the Structure and Function of W→F WW Domain Variants: Identification of a Natively Unfolded Protein That Folds upon Ligand Binding. *Biochemistry 38*, 14338–14351.
10. Kouvatsos, N., Meldrum, J. K., Searle, M. S., and Thomas, N. R. (2006) Coupling ligand recognition to protein folding in an engineered variant of rabbit ileal lipid binding protein. *Chem. Commun.,* 4623–4625.
11. Friedler, A., Veprintsev, D. B., Hansson, L. O., and Fersht, A. R. (2003) Kinetic instability of p53 core domain mutants: Implication for rescue by small molecules. *J. Biol. Chem. 278*, 24108–24112.
12. Friedler, A., and Fersht, A. R. (2004) Structural Distortion of p53 by the Mutation R249S and its Rescue by a Designed Peptide: Implications for "Mutant Conformation". *J. Mol. Biol. 336*, 187–196.
13. Boeckler, F. M., Joerger, A. C., Jaggi, G., Rutherford, T. J., Veprintsev, D. B., and Fersht, A. R. (2008) Targeted resue of a destabilised mutant of p53 by an in silici screened drug. *Proc. Natl. Acad. Sci. U.S.A. 105*, 10360–10365.
14. Lucke, C., Zhang, F., Ruterjans, H., Hamilton, J. A., and Sacchettini, J. C. (1996) Flexibility is a likely determinant of binding specificity in the case of ileal lipid binding protein. *Structure 4*, 785–800.
15. Hodsdon, M., and Cistola, D. P. (1997) Discrete Backbone Disorder in the Nuclear Magnetic Resonance Structure of Apo Intestinal Fatty Acid-Binding Protein: Implications for the Mechanism of Ligand Entry. *Biochemistry 36*, 1450–1460.
16. Corsico, B., Cistola, D. P., Frieden, C., and Storch, J. (1998) The helical domain of intestinal fatty acid binding protein is critical for collisional transfer of fatty acids to phospholipid membranes. *Proc. Natl. Acad. Sci. U.S.A. 95*, 12174–12178.
17. Corsico, B., Liou, H. L., and Storch, J. (2004) The α-helical domain of liver fatty acid binding protein is responsible for the diffusion-mediated transfer of a fatty acids to phospholipid membranes. *Biochemistry 43*, 3600–3607.
18. Corsico, B., Franchini, G. R., Hsu, K.-T., and Storch, J. (2005) Fatty acid transfer from intestinal fatty acid binding protein to membranes: Electrostatic and hydrophobic interactions. *J. Lipid Res. 46*, 1765–1772.
19. Lucke, C. F., Zhang, J. A., Hamilton, J. C., Sacchettini, J. C., and Ruterjans, H. (2000) Solution structure of ileal lipid binding protein in complex with glycocholate. *Eur. J. Biochem. 267*, 2929–2938.
20. Kurz, M., Brachvogel, V., Matter, H., Stengelin, S., Thuring, H., and Kramer, W. (2003) Insights into the bile acid transport system: The human ileal lipid binding protein-cholyltaurine complex and its comparison with homologous structures. *Proteins 50*, 312–328.
21. Kouvatsos, N., Thurston, V., Ball, K., Oldham, N. J., Thomas, N. R., and Searle, M. S. (2007) Bile acid interactions with rabbit ileal lipid binding protein and an engineered helixless variant reveal novel ligand binding properties of a versatile β-clam shell protein scaffold. *J. Mol. Biol. 371*, 1365–1377.
22. Kim, K., Cistola, D. P., and Frieden, C. (1996) Intestinal fatty acid binding protein: The structure and stability of a helix-less variant. *Biochemistry 35*, 7553–7558.
23. Steele, R. A., Emmert, D. A., Kao, J., Hodsdon, M. E., Frieden, C., and Cistola, D. P. (1998) The three dimensional structure of a helix-less variant of intestinal fatty acid binding protein. *Protein Sci. 7*, 1332–1339.
24. Cistola, D. P., Kim, K., Rogl, H., and Frieden, C. (1996) Fatty acid interactions with a helix-less variant of intestinal fatty acid binding protein. *Biochemistry 35*, 7559–7565.
25. Curto, L. M., Caramelo, J. J., and Delfino, J. M. (2005) Δ98Δ, a functional all β-sheet abridged form of intestinal fatty acid binding protein. *Biochemistry 44*, 13847–13857.
26. Ogbay, B., Dekoster, G. T., and Cistola, D. P. (2004) The NMR structure of a stable and compact all β-sheet variant of intestinal fatty acid binding protein. *Protein Sci. 13*, 1227–1237.
27. Fangjun, W., Corsico, B., Flach, C. R., Cistola, D. P., Storch, J., and Mendelsohn, R. (2001) Deletion of the helical motif in the intestinal fatty acid binding protein reduces its interactions with membrane monolayers: Brewster angle microscopy, IR reflection-absorption spectroscopy and surface pressure studeies. *Biochemistry 40*, 1976–1983.
28. Tochtrop, G. P., Richter, K., Tang, C., Toner, J. T., Covey, D. F., and Cistola, D. P. (2002) Energetics by NMR: Site-specific binding in a positively co-operative system. *Proc. Natl. Acad. Sci. U.S.A. 99*, 1847.
29. Tochtrop, G. P., Bruns, J. L., Tang, C., Covey, D. F., and Cistola, D. P. (2003) Steroid ring hydroxylation patterns govern co-operativity in human bile acid binding protein. *Biochemistry 42*, 11561–11567.
30. Toke, O., Monsey, J. D., DeKoster, G. T., Tochtrop, G. P., Tang, C., and Cistola, D. P. (2006) Determinants of co-operativity and site selectivity in human ileal bile acid binding protein. *Biochemistry 45*, 727–737.
31. Tochtrop, G. P., DeKoster, G. T., Covey, D. F., and Cistola, D. F. (2004) A single hydroxyl group governs ligand site selectivity in human ileal lipid bile acid binding protein. *J. Am. Chem. Soc. 126*, 11024–11029.
32. Onitsuka, M., Kamikubo, H., Yamazaki, Y., and Kataoka, M. (2008) Mechanism of induced folding: Both folding before binding and binding before folding can be realised in staphylococcal nuclease mutants. *Proteins 72*, 837–847.
33. Bosshard, H. R. (2001) Molecular recognition by induced-fit: How fit is the concept?. *News Physiol. Sci. 16*, 171–173.
34. Kuzmic, P. (1996) Program DYNAFIT for the Analysis of Enzyme Kinetic Data: Application to HIV Proteinase. *Anal. Biochem. 237*, 260–273.
35. AMBER 8.0 suite of programs (http://amber.scripps.edu/doc8/index.html).
36. Koradi, R., Billeter, M., and Wuthrich, K. (1996) MOLMOL: A program for display and analysis of macromolecular structures. *J. Mol. Graphics 14*, 51–55.
37. Capaldi, S., Saccomani, G., Fessas, D., Signorelli, M., Perduca, M., and Monaco, H. L. (2009) The X-ray structure of zebrafish (*Danio rerio*) ileal bile acid binding protein reveals the presence of binding sites on the surface of the protein molecule. *J. Mol. Biol. 385*, 99–116.
38. Eads, J., Sacchettini, J. C., Kromminga, A., and Goedon, J. I. (1993) *Escherichia coli*-derived rat intestinal fatty acid binding protein with myristate at 1.5 Å resolution and I-FABP Arg106Gln with bound oleate at 1.74 Å resolution. *J. Biol. Chem. 268*, 26375–26385.
39. Young, A. C., Scapin, G., Kromminga, A., Patel, S. B., Verkamp, J. H., and Sacchettini, J. C. (1994) Structural studies on human muscle fatty acid binding protein at 1.4 Å resolution: Binding interactions with three C18 fatty acids. *Structure 2*, 523–534.
40. Weikl, T. R., and von Deuster, C. (2009) Selected-fit versus induced-fit protein binding: Kinetic differences and mutational analysis. *Proteins 75*, 104–110.
41. Tsai, C. J., and Nussinov, R. (1999) Folding and binding cascades: Shifts in energy landscapes. *Proc. Natl. Acad. Sci. U.S.A. 96*, 9970–9972.
42. Nieslanik, B. S., Dabrowski, M. J., Lyon, R. P., and Atkins, W. M. (1999) Stopped-Flow Kinetic Analysis of the Ligand-Induced Coil-Helix Transition in Glutathione S-Transferase A1-1: Evidence for a Persistent Denatured State. *Biochemistry 38*, 6971–6980.
43. Toke, O., Monsey, J. D., and Cistola, D. P. (2007) Kinetic mechanism of ligand binding in human ileal bile acid binding protein as determined by stopped-flow fluorescence analysis. *Biochemistry 46*, 5427–5436.
44. Koshland, D. E. (1994) The lock and key principle and the induced fit theory. *Angew. Chem., Int. Ed. 33*, 2475.
45. Shoemaker, B. A., Portman, J. J., and Wolynes, P. G. (2000) Speeding molecular recognition by using the folding funnel: The fly-casting mechanism. *Proc. Natl. Acad. Sci. U.S.A. 97*, 8868–8873.
46. Levy, Y., Onuchic, J. N., and Wolynes, P. G. (2007) Fly-casting in protein-DNA binding: Frustration between protein folding and electrostatics facilitates target recognition. *J. Am. Chem. Soc. 129*, 738–739.
47. Onuchic, J. N., Luthey-Schulten, Z., and Wolynes, P. G. (1997) Theory of protein folding: The energy landscape perspective. *Annu. Rev. Phys. Chem. 48*, 545–600.
48. Crespin, M. O., Boys, B. L., and Konermann, L. (2005) The reconstitution of unfolded myoglobin with hemin dicyanide is not accelerated by fly-casting. *FEBS Lett. 579*, 271–274.
49. Dalessio, P. M., and Ropson, I. J. (2000) β-Sheet proteins with nearly identical structures have different folding intermediates. *Biochemistry 39*, 860–871.